Diamond & Related Materials 119 (2021) 108597

Contents lists available at ScienceDirect

Diamond & Related Materials

journal homepage: www.elsevier.com/locate/diamond

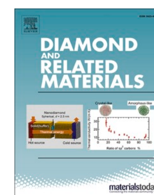

A monolithic, back-gated diamond field-effect transistor for tunable color centers

D. Oing [a,*], M. Ney [a], G. Bendt [b], S. Schulz [b], M. Geller [a], N. Wöhrl [a], A. Lorke [a]

[a] Department of Physics and CENIDE, University Duisburg-Essen, Lotharstr. 1, 47057 Duisburg, Germany
[b] Faculty of Chemistry, Inorganic Chemistry and CENIDE, University of Duisburg-Essen, Universitätsstr. 7, D-45114 Essen, Germany

ARTICLE INFO

Keywords:
Two-dimensional hole gas
Single crystal diamond
P-type doping
Surface electronic properties
Boron doping
Field effect transistor
Nitrogen-vacancy center

ABSTRACT

We present an innovative design for a monolithic field effect transistor, where all components consist of the wide-bandgap material diamond. The back gate-electrode is realized by a buried, degenerately boron-doped diamond (resistivity $< 10^{-2}\ \Omega$ cm), while the dielectric material is made of lightly nitrogen-doped diamond. The 2DHG on the hydrogen-terminated surface serves as the conductive channel of the transistor. We discuss the band structure of this device, the function of each individual component and show the sample preparation routine. Furthermore, we investigate the electrical tunability of the 2DHG and the optical tunability of NV-centers in a first proof-of-principle sample. Additionally, we use the field effect to manipulate the charge state of color centers in the nitrogen-doped film. This vertical and monolithic device structure opens up a range of applications, not only in the diamond semiconductor and quantum information technology, but also for sensing applications where the back-gating is advantageous or where an all-diamond layer sequence is beneficial.

1. Introduction

Diamond is a promising wide-bandgap semiconductor for harsh environments [1,2], power applications [3] and for high frequency devices [4]. This is due to its extraordinary properties like the highest thermal conductivity up to 2200 W/mK [5], an electric breakdown field of up to 13 MV/cm [6] and high electron and hole mobilities of 3800 cm^2/Vs and 4500 cm^2/Vs [7], respectively.

Doping in diamond is typically achieved using boron as electron acceptor (p-type dopant) [8] and phosphorus as electron donor (n-type dopant) [9]. Unfortunately, these dopants have high activation energies that lead to a small ionization yield even at room temperature. However, hydrogen termination of the diamond surface and exposure to ambient atmosphere leads to the formation of a two-dimensional hole gas (2DHG) [10], and carrier concentrations up to $1.5 \cdot 10^{13} cm^{-2}$ can be achieved [11] with negligible temperature dependence.

In contrast to traditional devices, which use metal oxides as dielectric material [12–17], we herein present a monolithic field-effect transistor (FET) exclusively made of diamond. The 2DHG on the diamond surface is used as channel, diamond as dielectric material, and degenerately boron-doped diamond as buried gate in this FET structure. This monolithic diamond-based FET shows several advantages to classical designs that combine different materials, i.e., superior properties of diamond used as a dielectric material such as the high breakdown field and the high thermal conductivity. Additionally, the H-terminated surface stays accessible as an interface for sensor applications, e.g. for electrochemical and biological systems [18–21]. Furthermore, this device structure allows to change the charge state of color centers in diamond by applying a gate voltage, similar to previous studies in Refs [22–24].

2. Device design and tailored band structure

Fig. 1a illustrates the main device concept, which consists of three layers: (i) a degenerately boron-doped layer used as metallic back gate, (ii) a lightly nitrogen-doped layer used as a dielectric barrier and (iii) the 2DHG on the surface that is used as the transistor channel. In the following, based on this layer sequence (which also reflects the growth direction), the different layers and their influence on the band structure will be discussed.

The mentioned structure is similar to a previously presented structure in Reference [22], where a degenerately boron-doped layer is used as a buried metallic contact. However, in the present study, we use the 2DHG on diamond instead of a metallic contact on the diamond surface. The different shaped band structure is suitable as a field effect transistor.

* Corresponding author.
E-mail address: dennis.oing@uni-due.de (D. Oing).

https://doi.org/10.1016/j.diamond.2021.108597
Received 27 July 2021; Received in revised form 27 August 2021; Accepted 3 September 2021
Available online 8 September 2021
0925-9635/© 2021 Elsevier B.V. All rights reserved.

To calculate the band structure, the doping concentration of the different layers, shown in Fig. 1b, is decisive. The buried gate is degenerately boron-doped with a concentration of 7 • 10^{20} cm^{-3} [8,25]. Its nitrogen background concentration was estimated to be as low as 10^{15} cm^{-3}.

In this calculation, the second layer is divided in 180 nm with a nitrogen doping of 6.36 • 10^{16} cm^{-3} and a 22 nm layer where the nitrogen doping concentration is decreased (see Fig. 1b). Section 3, below, explains the details and corresponding calculations to get this nitrogen doping concentration.

Based on this doping profile and the freeware software "1D-Poisson Solver" [26] the band structure, the hole concentration and the electric field were calculated (Fig. 1c–e).

Note that the band structure (Fig. 1c) and therefore the hole concentration (Fig. 1d) strongly depends on the nitrogen concentration in the dielectric layer. These nitrogen n-type dopants are used as counter doping for holes in the dielectric layer which are formed due to the boron doped layer and the 2DHG, both layers being p-type. To achieve a decent dielectric material with a sufficient high resistance between the 2DHG and the boron-doped diamond, an adequate nitrogen concentration is required. The expected specific resistance between the degenerately doped layer and the 2DHG can be calculated using

$$\rho = \int \frac{1}{ep(z)\mu} \mathrm{d}z. \tag{1}$$

Here, $p(z)$ is the hole concentration shown in Fig. 1d.

3. Sample preparation

In the following paragraph, we will show the sample preparation methods and demonstrate the usability of such a device as a field-effect transistor that has the potential to measure and manipulate the charge state of an incorporated nitrogen-vacancy center (NV-center). The sample was grown in custom-made microwave plasma enhanced CVD reactor including an iplas CYRANNUS plasma source and using a HPHT-(100) oriented substrate from ElementSix with a size of 3 • 3 mm^2. The monolithic diamond FET on the sample was grown in two different CVD steps.

First, a boron-doped layer was grown using tripropyl borane ($(C_3H_7)_3B$) as a dopant. This liquid precursor is placed in a vacuum-sealed bottle, evaporated and fed into the CVD chamber via an argon carrier gas. The following growth parameters were applied: a gas pressure of 141 mbar, microwave power of 2.4 kW, a substrate temperature of 830 °C and a gas flow of 384 sccm H_2, 16 sccm CH_4 and 30 sccm Ar. Our experiments show that the sequence in which the gases are added to the process has an important influence on the morphology of the grown diamond layers. Since the morphology has a strong influence on the conductivity of the 2DHG and on the breakdown electric field strength, special care was taken to find process parameters that led to good material properties. Hence, a growth process of 6 min with tripropyl borane was performed after 3 min growth with methane diluted in hydrogen. Electrical characterizations of these layers show that the doping concentration can be as high as 9.4 • $10^{20}$$cm^{-3}$ with a typical specific

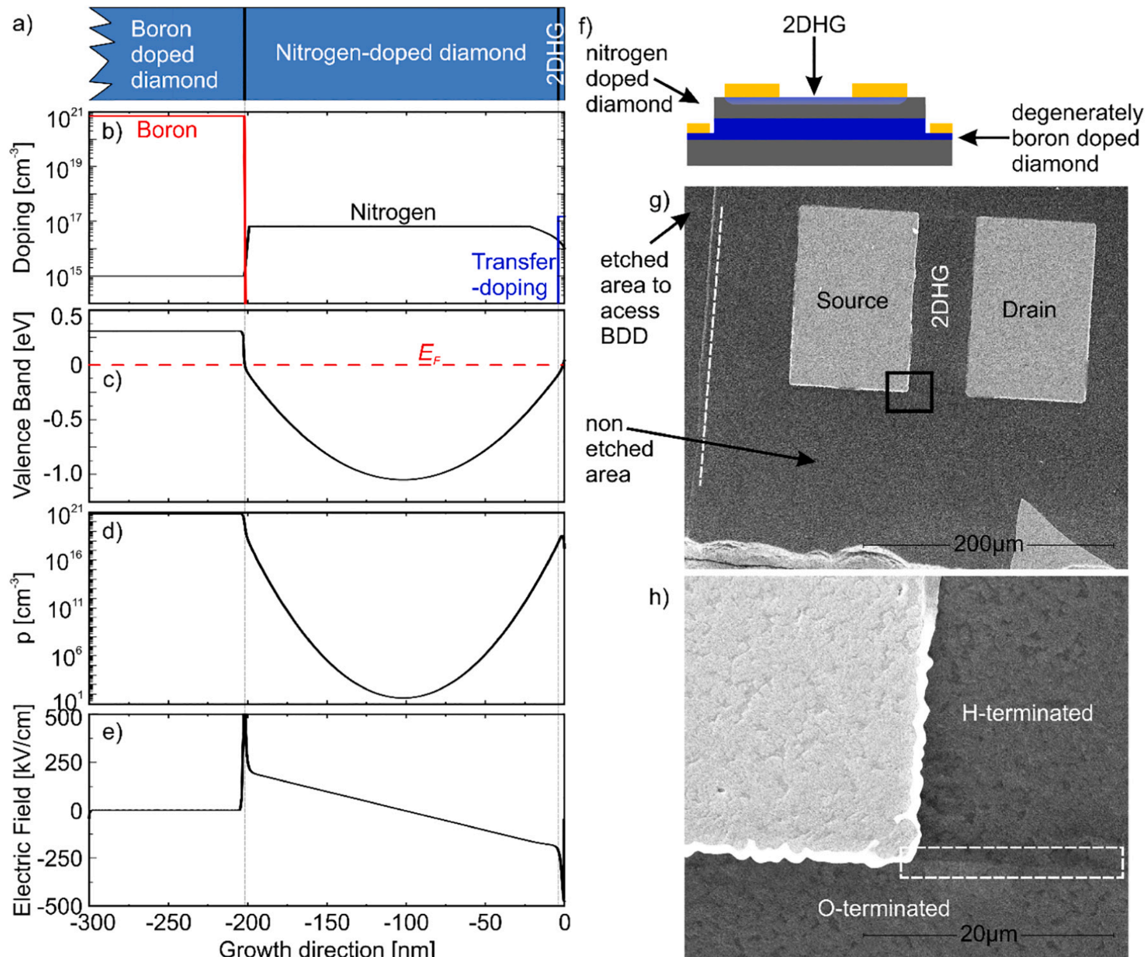

Fig. 1. a) Stacking sequence, b) doping profile, c) valence band, d) hole concentration and e) intrinsic electric field of the diamond FET. f) Schematic representation of the final device. g) Scanning electron microscopy picture of the surface of the final device. h) Enlarged picture of the surface to verify the transition between H-terminated and O-terminated surface.

resistance below 10^{-2} Ω cm. As already reported by other groups, this doping concentration is high enough to be considered as metallic, degenerate doping [8,25].

In a second step, a nitrogen-doped layer was grown on top of the boron-doped layer. This growth step was performed in a different reactor to avoid boron cross contamination [27–29]. The growth conditions were a gas pressure of 111 mbar, a microwave power of 1.06 kW, a substrate temperature of 720 °C and a mixture of 8 sccm CH_4 and 250 ppm nitrogen diluted in 392 sccm hydrogen. This was executed for 9 min with a growth rate of 20 nm/min before the nitrogen supply was switched off and the growth was continued for 1.5 min. This was done to decrease the nitrogen concentration at the diamond surface as nitrogen donors at the surface are known to suppress the formation of the 2DHG [30]. Using the residence time of gas species in the plasma assisted CVD reaction chamber we calculated the expected decrease in nitrogen concentration in the gas phase during the deposition process [31,32]. Additionally, this decrease is monitored by the CN signal of optical emission spectroscopy. Utilizing Eq. (1), we were able to calculate the nitrogen concentration in the final device from the measured resistance (see Ohmic behavior in Fig. 2c). Taking the nitrogen concentration of 250 ppm in the gas phase, we calculated an incorporation rate of $3.6 \bullet 10^{-4}$ for nitrogen into the diamond, in good agreement with incorporation rates reported in the literature [33,34].

To realize the electrical contact to the back gate, the sample was subsequently etched down to the boron doped layer at all four corners using reactive-ion etching (RIE) in an inductively coupled radio frequency plasma. Aluminum was used as a hard mask. Plasma etching was performed with a gas pressure of $2.2 \bullet 10^{-1}$ mbar, a power of 800 W, a substrate temperature of 360 °C, a bias voltage of 104 V with a gas flow of 40 sccm O_2 and 80 sccm Ar for 9 min. This etching step removes 270 nm of diamond. Afterwards, the aluminum was removed in NaOH.

Metallization was achieved by using standard photolithography. Two contacts on the H-terminated surface with an area of $150 \bullet 100\ \mu m^2$ and a distance of 50 μm, consisting of 12 nm NiCr as adhesion layer and 63 nm Au, were deposited. The H-termination outside of the transistor area was selectively removed in a short oxygen plasma treatment as described in Ref [11]. Fig. 1f shows a schematic representation of the finished device. Fig. 1g and h show SEM images of the surface of the device, where the expected contrast difference between O-terminated and H-terminated surface is discernible.

4. Electrical characterization

The measured capacitance of the transistor is about 9 pF at zero gate voltage, $V_g = 0$. Using the model of a plate capacitor, the area of the 2DHG (50 μm × 150 μm) and the dielectric constant of $\varepsilon_r = 5.7$ for diamond [6], we calculate a capacitor plate distance of 202.1 nm, which is in good agreement with the expected film thickness from the growth procedure.

Fig. 2a shows the current-voltage characteristics between the source-drain contacts for gate voltages ranging from -13 V to +4 V. In the measured regime, the leakage current through the gate contact was below 1 nA. This low vertical leakage current through the gate demonstrates that the nitrogen-doped region is fully depleted (and insulating) so that the lateral transport through the 2DHG is not affected by any parallel current through the bulk diamond layer.

Fig. 2b shows the transconductance of the device for a constant source drain voltage of 4 V. Using a linear extrapolation, we find a threshold voltage of V_{th} = -4.7 V. Additionally, we calculate a field-effect mobility of 0.06 cm^2/Vs which is three orders of magnitude lower than mobilities measured on diamond [11]. The reason is presumably the non-optimized growth of the nitrogen-doped layer as indicated by the broadening of the 1332 cm^{-1} diamond Raman peak with a FWHM of 14.3 cm^{-1} (not shown here), while the degenerately boron-doped layer shows a Raman peak with a FWHM of 5 cm^{-1}.

Fig. 2c shows the current-voltage characteristic between the 2DHG and the boron-doped layer (gate). In the gate voltage region between -12.4 V and +10 V, we determine a high resistance of 98 GΩ, which demonstrates that the nitrogen counter doped layer serves as a suitable dielectric with low leakage. The breakdown voltage was determined to be V_{bd} = -14.7 V, which corresponds to a breakdown field of 725 kV/cm. This is more than one order of magnitude lower than the maximum breakdown voltage of diamond. We again assign this to the relatively low quality of the single crystal diamond dielectric layer indicated by the broadened diamond Raman peak signal. However, this breakdown voltage allows to tune the carrier density from 0 to $2,4 \bullet 10^{12} cm^{-2}$ with a field effect. Despite the poor mobility of the 2DHG, the presented device is a fully functional p-type enhancement-mode FET.

5. Electrical tuning of NV-centers, embedded in a transistor structure

As the dielectric material was grown with nitrogen as counter doping (doping concentration $6.36 \bullet 10^{16}$, see Section 2) we expect it to contain nitrogen-vacancy centers (NV-centers). Therefore, we performed low-temperature micro-photoluminescence, where some nitrogen donors are transformed to NV-centers. Ref. [34] shows a conversion from nitrogen to NV^- of around 0.36%. With a laser spot diameter of approx. 1 μm on the diamond surface and a transistor thickness of 202.1 nm, we can expect to measure an ensemble of ~75 NV-centers simultaneously in our experimental setup. Note, that the used conversion rate is for the negative charge state, and we expect that this density for all NV-center

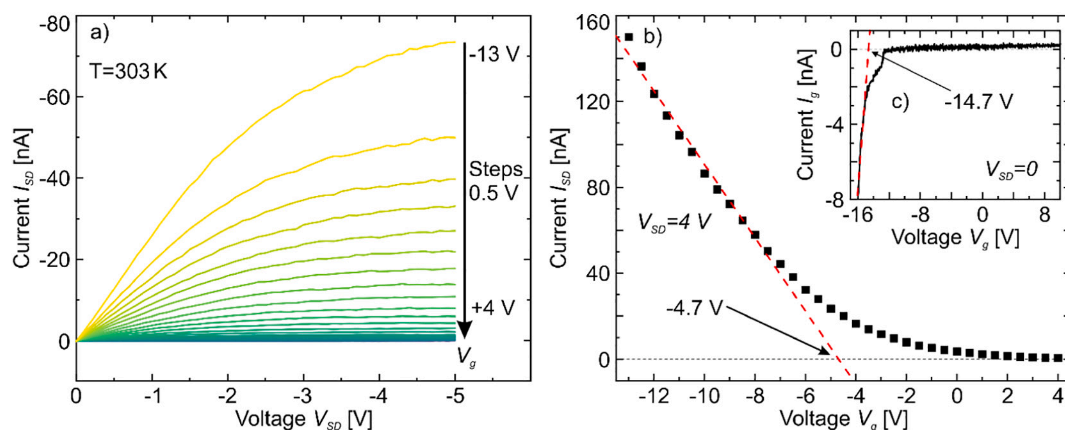

Fig. 2. a) IV-characteristics for on applied gate-voltages between V_g = -13 V and +4 V in 0.5 V steps. b) Transconductance with a threshold voltage of V_{th} = -4.7 V. c) Leakage current with a breakdown voltage of -14.7 V.

charge states (NV^+, NV^0 and NV^-) is even higher.

Typical PL spectra are shown in Fig. 3a. Two broad maxima can be observed from the neutral (at 2.16 eV) and the negatively charged (at 1.94 eV) NV-centers. The FWHM of these PL maxima are 12.5 meV and 17.8 meV for the NV^0 and the NV^-, respectively, broader in energy than the FWHM observed, e.g. by Tamarat et al. [35]. This broad NV-center emission may have the following reasons: (i) The quality of the nitrogen-doped single crystal diamond layer is low, as already mentioned. (ii) The nitrogen donors in the dielectric barrier are fully ionized as they act as counter doping. This leads to Coulomb interaction and reduces the life time of the excited states. (iii) A possible differently pronounced Stark shift in the ensemble due to the built-in electric field of the device (Fig. 1e).

To further investigate the Stark shift, we applied an electric field using the gate voltage. The calculated Stark shift for both charge states of the NV-center is shown in Fig. 3b. We observe a Stark shift of 2.5 μeV/kV cm^{-1} for the neutral charge state NV^0 and 3.6 μeV/kV cm^{-1} for the negative charge state NV^- at 85 K in the linear region of Fig. 3b (black and red line). This is in good agreement with observed Stark shifts of 2.6 μeV/kV cm^{-1} measured on a single color-center in diamond [36]. By taking the electric field as shown in Fig. 1e, we find that about 17% of the FWHM can be attributed to the Stark shift.

Furthermore, we also investigated the charge state of the ensemble of NV-centers below our excitation laser spot. As seen in Fig. 4a, the intensity of both charge states increases with increasing gate voltage from V_g = -14 V to +4 V. This behavior could be explained for the NV^--center using the Fowler-Nordheim tunneling (FNT) process. The excited state ^3E of the NV^--center (see Fig. 4c) is quenched by FNT for gate voltages of V_g < -9 V (see below for further discussion) and, hence, the photoluminescence intensity decreases accordingly.

In more detail, in equilibrium with no laser excitation, we do not expect to observe the negative charge state as the dielectric layer is depleted and there are no free electrons to form the NV^- state. Therefore, the luminescence from NV^- states in Fig. 4a is explained by photoconversion [36,37], where electrons are optically-excited from the valence band into the NV-center by the photoelectric effect. Hence, the density of NV^--centers depends on two factors: (i) the density of NV^0-centers (which is also manipulated by the applied gate voltage) and (ii) optical photoconversion by the laser excitation power. The laser power is constant at 500 μW in the experiment shown in Fig. 4a. However, we have performed measurements at lower excitation power of 50 μW (not shown here), where the overall intensities of the optical transitions of

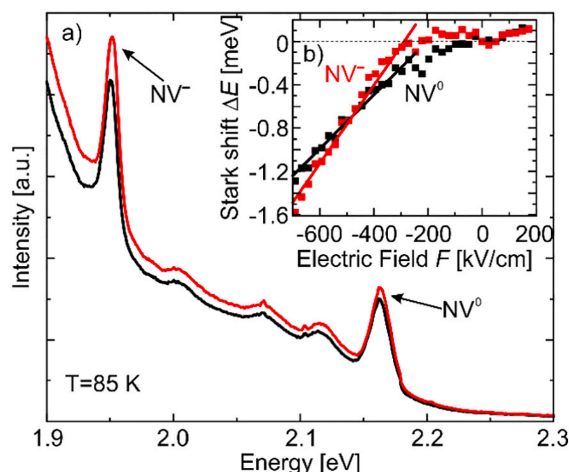

Fig. 3. a) Photoluminescence spectra at 85 K for a gate Voltage of V_g = -14 V (black) and -9 V (red) with a laser excitation power of 500 μW. b) Stark shift of the neutrally- (black) and negatively-charged NV-centers (red). (For interpretation of the references to color in this figure legend, the reader is referred to the web version of this article.)

the NV^-- and NV^0-centers are decreased and the NV^-/NV^0-intensity ratio has lowered, supporting the photoconversion picture. According to (i), the intensity of the NV^- transition increases the same way as the NV^0 intensity in Fig. 4a for increasing gate voltage. Furthermore, the intensity ratio for both charge states is constant as far as the laser intensity is kept constant. However, this is only true for $V_g > -9$ V as shown in Fig. 4b (black squares). For lower gate voltages ($V_g < -9$ V) the intensity of the NV^- is reduced due to an electron tunneling process from the NV^--center into the conduction band of diamond. For high negative gate voltage, the band structure is heavily tilted and the distance between the conduction band minimum and the ^3E excited state of the NV^--center is decreased as depicted in Fig. 4c. To calculate the tunneling probability, we assume a triangular barrier, where now FNT can occur. The FNT is given by [40]

$$J(V_g) = \frac{e^2F^2}{16\pi^2\hbar V_0} exp\left(-\frac{4}{3}\frac{\sqrt{2mV_0^3}}{\hbar eF}\right) \tag{2}$$

Here, F is the electric field (see Fig. 1e) and V_0 is the barrier height. The barrier height of 0.6 eV is given by the distance between ^3E and conduction band minimum [41]. The distance d is solely given by the band structure. The calculated tunneling probability is shown in the red curve of Fig. 4b and fits very good to measured values. The tunneling probability is anti-proportional to the decrease in intensity of NV^-/NV^0 ratio. This demonstrates that the decrease in the intensity for NV^--center is a result of electron tunneling from ^3E into the conduction band before the excited state could decay radiatively.

Also visible in Fig. 4a is the intensity decrease of the NV^0 transition that almost follows the behavior of the NV^- transition. However, FNT cannot explain this behavior as the gate voltage dependent tunneling probability for the ground and the excited states of NV^0 are negligible; estimated by using Eq. (2). From this estimation we have to conclude that an additional effect takes place. Possible effects are: (i) By photoconversion the charge states are transferred from $NV^+ \rightarrow NV^0 \rightarrow NV^-$ and vice versa. By reducing the numbers of centers in the NV^--state by FNT, this equilibrium is disturbed. (ii) By applying a negative gate voltage the NV^0, centers are transformed into NV^+ state, due to the high hole density in the 2DHG [38,39] or (iii) due to the energy levels shifting above the Fermi-level by applying a gate voltage. However, further investigations are needed to understand the increase of the intensity of the NV^0 for increasing gate voltage in Fig. 4a.

6. Summary and outlook

A novel vertical transistor structure solely made from doped diamond is fabricated and the band structure and the importance of the doping profile discussed. It is demonstrated that this device can be used for field effect applications, such as a p-type enhancement-mode FET and for color center applications.

The presented device structure is promising for future work as it opens up a new field of research for color centers in diamond. Color centers can be selectively implemented into this structure, e.g. SiV by ion implantation. These color centers can be coupled to the 2DHG and using the conductance of the 2DHG as sensor allows it to electrically read out the color centers charge state, a technique that has successfully been implemented to study single electron dynamics in quantum dots [42].

CRediT authorship contribution statement

D. O., M. G., N. W. and A. L. conceived of the presented idea. D.O. and A.L. developed the presented band structure.

D. O., G. B. and S. S. contributed to the sample preparation presented in the study. D. O. and M. N. carried out the experiments. D. O., M. G., N. W. and A. L. evaluated the data.

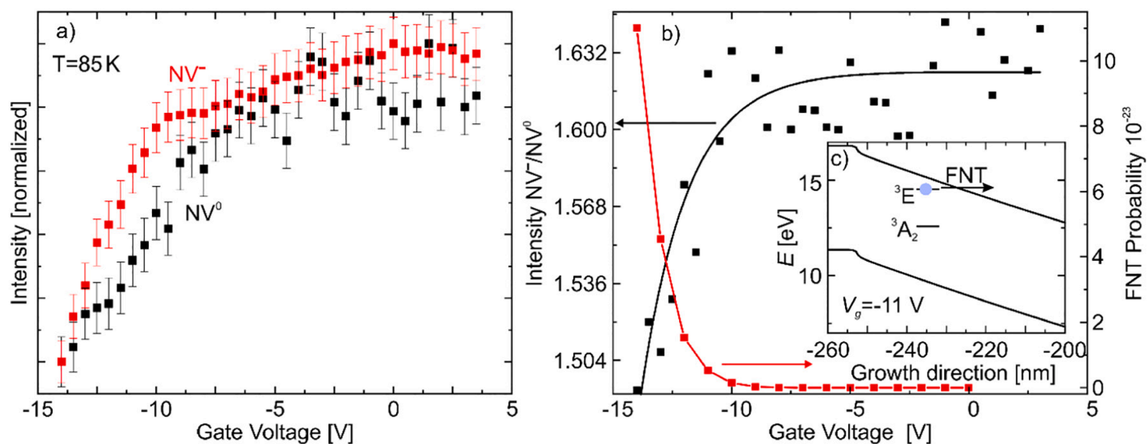

Fig. 4. a) Gate voltage dependence of the normalized intensities for both charge states of the NV-center. b) Ratio NV^-/NV^0 for a gate voltage between V_g = -14 V and +4 V (black squares). The black line is a guide to the eye. The red squares are calculated as probability from a Fowler-Nordheim tunnel process. c) Schematic picture of the Fowler-Nordheim tunnel (FNT) process of an electron tunneling from the ^3E-state into the conduction band of diamond (at a gate voltage of V_g = -11 V). (For interpretation of the references to color in this figure legend, the reader is referred to the web version of this article.)

All authors provided critical feedback and helped shape the manuscript.

Declaration of competing interest

The authors declare that they have no known competing financial interests or personal relationships that could have appeared to influence the work reported in this paper.

Acknowledgements

This work was funded by the Deutsche Forschungsgemeinschaft (DFG, German Research Foundation) – Project-ID 278162697 – SFB 1242.

References

[1] S. Baccaro, A. Cemmi, I.D. Sarcina, B. Esposito, G. Ferrara, A. Grossi, M. Montecchi, S. Podda, F. Pompili, L. Quintieri, M. Riva, Radiation damage tests on diamond and scintillation detector components for the ITER radial neutron camera, IEEE Trans. Nucl. Sci. 65 (2018) 2046–2053, https://doi.org/10.1109/tns.2018.2807841.
[2] G.H. Kroetz, M.H. Eickhoff, H. Moeller, Silicon compatible materials for harsh environment sensors, Sensors Actuators 74 (1999) 182–189, https://doi.org/10.1016/s0924-4247(98)00296-9.
[3] G. Perez, A. Marechal, G. Chicot, P. Lefrance, P.-O. Jeannin, D. Eon, N. Rouger, Diamond semiconductor performances in power electronics applications, Diam. Relat. Mater. 108154 (2020), https://doi.org/10.1016/j.diamond.2020.108154.
[4] H. Kawarada, High-current metal oxide semiconductor field-effect transistors on H-terminated diamond surfaces and their high-frequency operation, Jpn. J. Appl. Phys. 51 (2012), 090111, https://doi.org/10.1143/jjap.51.090111.
[5] J.E. Field, The Properties of Natural and Synthetic Diamond, Academic Press, New York, 1992.
[6] M.W. Geis, T.C. Wade, C.H. Wuorio, T.H. Fedynyshyn, B. Duncan, M.E. Plaut, J. O. Varghese, S.M. Warnock, S.A. Vitale, M.A. Hollis, Progress toward diamond power field-effect transistors, Phys. Status Solidi A 215 (2018) 1800681, https://doi.org/10.1002/pssa.201800681.
[7] J. Isberg, J. Hammersberg, E. Johansson, T. Wikstro, D.J. Twitchen, A. J. Whitehead, S.E. Coe, G.A. Scarsbrook, High carrier mobility in single-crystal plasma-deposited diamond, Science 297 (2002) 1670, https://doi.org/10.1126/science.1074374.
[8] J. Achard, F. Silva, R. Issaoui, O. Brinza, A. Taillaire, H. Schneider, K. Isoird, H. Ding, S. Kone, M.A. Pinault, F. Jomard, A. Gicquel, Thick boron doped diamond single crystals for high power electronics, Diam. Relat. Mater. 20 (2011) 145–152, https://doi.org/10.1016/j.diamond.2010.11.014.
[9] E. Gheeraert, S. Koizumi, T. Teraji, H. Kanda, Electronic transitions of electrons bound to phosphorus donors in diamond, Solid State Commun. 113 (2000) 577–580, https://doi.org/10.1016/s0038-1098(99)00546-3.
[10] F. Maier, M. Riedel, B. Mantel, J. Ristein, L. Ley, Origin of surface conductivity in diamond, Phys. Rev. Lett. 85 (2000) 3472–3475, https://doi.org/10.1103/physrevlett.85.3472.
[11] D. Oing, M. Geller, A. Lorke, N. Wöhrl, Tunable carrier density and high mobility of two-dimensional hole gases on diamond: the role of oxygen adsorption and surface roughness, Diam. Relat. Mater. 97 (2019), 107450, https://doi.org/10.1016/j.diamond.2019.107450.
[12] T. Saito, K. Park, K. Hirama, H. Umezawa, M. Satoh, H. Kawarada, Z. Liu, K. Mitsuishi, K. Furuya, H. Okushi, Fabrication of metal–oxide–diamond field-effect transistors with submicron-sized gate length on boron-doped (111) H-terminated surfaces using electron beam evaporated SiO2 and Al2O3, J. Electron. Mater. 40 (2011) 247–252, https://doi.org/10.1007/s11664-010-1500-1.
[13] J.W. Liu, M.Y. Liao, M. Imura, H. Oosato, E. Watanabe, Y. Koide, Electrical characteristics of hydrogen-terminated diamond metal-oxide-semiconductor with atomic layer deposited HfO2 as gate dielectric, Appl. Phys. Lett. 102 (2013), 112910, https://doi.org/10.1063/1.4798289.
[14] K. Hirama, H. Sato, Y. Harada, H. Yamamoto, M. Kasu, Diamond field-effect transistors with 1.3A/mm drain current density by Al2O3 passivation layer, Jpn. J. Appl. Phys. 51 (2012), 090112, https://doi.org/10.1143/jjap.51.090112.
[15] H. Kawarada, T. Yamada, D. Xu, H. Tsuboi, Y. Kitabayashi, D. Matsumura, M. Shibata, T. Kudo, M. Inaba, A. Hiraiwa, Durability-enhanced two dimensional hole gas of C-H diamond surface for complementary power inverter applications, Sci. Rep. 7 (2017), https://doi.org/10.1038/srep42368.
[16] J.W. Liu, H. Oosato, M.Y. Liao, Y. Koide, Enhancement-mode hydrogenated diamond metal-oxide-semiconductor field-effect transistors with Y2O3 oxide insulator grown by electron beam evaporator, Appl. Phys. Lett. 110 (2017), 203502, https://doi.org/10.1063/1.4983091.
[17] K.G. Crawford, J.D. Weil, P.B. Shah, D.A. Ruzmetov, M.R. Neupane, K. Kingkeo, A. Glen Birdwell, T.G. Ivanov, Diamond field-effect transistors with V2O5-induced transfer doping: scaling to 50-nm gate length, IEEE Trans. Electron Devices 67 (2020) 2270–2275, https://doi.org/10.1109/ted.2020.2989736.
[18] K. Takahashi, M. Tanga, O. Takai, H. Okamura, DNA preservation using diamond chips, Diam. Relat. Mater. 12 (2003) 572–576, https://doi.org/10.1016/s0925-9635(03)00070-0.
[19] W. Yang, O. Auciello, J.E. Butler, W. Cai, J.A. Carlisle, J.E. Gerbi, D.M. Gruen, T. Knickerbocker, T.L. Lasseter, J.N. Russell Jr., L.M. Smith, R.J. Hamers, DNA-modified nanocrystalline diamond thin-films as stable, biologically active substrates, Nat. Mater. 1 (2002) 253–257, https://doi.org/10.1038/nmat779.
[20] K.-Y. Tse, B.M. Nichols, W. Yang, J.E. Butler, J.N. Russell Jr., R.J. Hamers, Electrical properties of diamond surfaces functionalized with molecular monolayers, J. Phys. Chem. B 109 (2005) 8523, https://doi.org/10.1021/jp046433w.
[21] A. Härtl, E. Schmich, J.A. Garrido, J. Hernando, S.C.R. Catharino, S. Walter, P. Feulner, A. Kromka, D. Steinmueller, M. Stutzmann, Protein-modified nanocrystalline diamond thin films for biosensor applications, Nat. Mater. 3 (2004) 736, https://doi.org/10.1038/nmat1204.
[22] M. Krecmarová, M. Gulka, T. Vandenryt, J. Hrubý, L. Fekete, P. Hubík, A. Taylor, V. Mortet, R. Thoelen, E. Bourgeois, M. Nesládek, A label-free diamond microfluidic DNA sensor based on active nitrogen-vacancy center charge state control, ACS Appl. Mater. Interfaces 13 (16) (2021) 18500–18510, https://doi.org/10.1021/acsami.1c01118.
[23] M. Pfender, N. Aslam, P. Simon, D. Antonov, G. Thiering, S. Burk, F. Favaro de Oliveira, A. Denisenko, H. Fedder, J. Meijer, J.A. Garrido, A. Gali, T. Teraji, J. Isoya, M.W. Doherty, A. Alkauskas, A. Gallo, A. Grüneis, P. Neumann, J. Wrachtrup, Protecting a diamond quantum memory by charge state control, Nano Lett. 17 (10) (2017) 5931–5937, https://doi.org/10.1021/acs.nanolett.7b01796.
[24] Y. Doi, T. Makino, H. Kato, D. Takeuchi, M. Ogura, H. Okushi, H. Morishita, T. Tashima, S. Miwa, S. Yamasaki, P. Neumann, J. Wrachtrup, Y. Suzuki, N. Mizuochi, Deterministic electrical charge-state initialization of single nitrogen-vacancy center in diamond, Phys. Rev. X 4 (2014), 011057, https://doi.org/10.1103/PhysRevX.4.011057.

[25] P. Volpe, J. Arnault, N. Transchant, G. Chicot, J. Pernot, F. Jomard, P. Bergonzo, Boron incorporation issues in diamond when TMB is used as precursor: toward extreme doping levels, Diam. Relat. Mater. 22 (2012) 136–141, https://doi.org/10.1016/j.diamond.2011.12.019.

[26] https://www3.nd.edu/~gsnider/.

[27] P. Hartmann, S. Bohr, R. Haubner, B. Lux, P. Wurzinge, M. Griesser, A. Bergmaier, G. Dollinger, H. Sternschulte, R. Sauer, Diamond growth with boron addition, Int. J. Refract. Met. Hard Mater. 16 (1998) 223–232, https://doi.org/10.1016/s0263-4368(98)00022-5.

[28] V. Mortet, J. Pernot, F. Jonard, A. Soltani, Z. Remes, J. Barjon, J. D'Haen, K. Haenen, Properties of boron-doped epitaxial diamond layers grown on (110) oriented single crystal substrates, Diam. Relat. Mater. 53 (2015) 29–34, https://doi.org/10.1016/j.diamond.2015.01.006.

[29] A.F. Sartori, M. Fischer, S. Gsell, M. Schreck, In situ boron doping during heteroepitaxial growth of diamond on Ir/YSZ/Si, Phys. Status Solidi (a) 209 (9) (2012) 1643–1650, https://doi.org/10.1002/pssa.201200221.

[30] J. Ristein, M. Riedel, F. Maier, B.F. Mantel, M. Stammler, L. Ley, Surface conductivity of diamond as a function of nitrogen doping, Phys. Status Solidi A 186 (2) (2001) 249–256, https://doi.org/10.1002/1521-396x(200108)186:2<249::aid-pssa249>3.0.co;2-6.

[31] T. Kobayashi, K.K. Hirakuri, N. Mutsukura, Y. Machi, Synthesis of CVD diamond at atmospheric pressure using the hot-filament CVD method, Diam. Relat. Mater. 8 (1999) 1057–1060, https://doi.org/10.1016/s0925-9635(99)00093-x.

[32] E. Nakamura, K.K. Hirakuri, M. Ohyama, G. Friedbacher, N. Mutsukura, High quality chemical vapor deposition diamond growth on iron and stainless steel substrates, J. Appl. Phys. 6 (2002) 3393–3396, https://doi.org/10.1063/1.1502917.

[33] S. Jin, T.D. Moustakas, Effect of nitrogen on the growth of diamond films, Appl. Phys. Lett. 65 (1994) 403, https://doi.org/10.1063/1.112315.

[34] A. Tallaire, A. Collins, D. Charles, J. Achard, R. Sussmann, A. Gicquel, M. Newton, A. Edmonds, R. Cruddace, Characterisation of high-quality thick single-crystal diamond grown by CVD with a low nitrogen addition, Diam. Relat. Mater. 15 (2006) 1700, https://doi.org/10.1016/j.diamond.2006.02.005.

[35] P. Tamarat, T. Gaebel, J.R. Rabeau, M. Khan, A.D. Greentree, H. Wilson, L.C. L. Hollenberg, S. Prawer, P. Hemmer, F. Jelezko, J. Wrachtrup, Stark shift control of single optical centers in diamond, Phys. Rev. Lett. 97 (2006), 083002, https://doi.org/10.1103/physrevlett.97.083002.

[36] M.W. Doherty, N.B. Manson, P. Delaney, F. Jelezko, J. Wrachtrup, L.C. L. Hollenberg, The nitrogen-vacancy colour centre in diamond, Phys. Rep. 528 (1) (2013), https://doi.org/10.1016/j.physrep.2013.02.001.

[37] P. Siyushev, M. Nesladek, E. Bourgeois, M. Gulka, J. Hruby, T. Yamamoto, M. Trupke, T. Teraji, J. Isoya, F. Jelezko, Photoelectrical imaging and coherent spin-state readout of single nitrogen-vacancy centers in diamond, Science 363 (2019) 728–731, https://doi.org/10.1126/science.aav2789.

[38] M.V. Hauf, P. Simon, N. Aslam, M. Pfender, P. Neumann, S. Pezzagna, J. Meijer, J. Wrachtrup, M. Stutzmann, F. Reinhard, J.A. Garrido, Addressing single nitrogen-vacancy centers in diamond with transparent in-plane gate structures, Nano Lett. 14 (2014) 2359–2364, https://doi.org/10.1021/nl4047619.

[39] C. Schreyvogel, V. Polyakov, R. Wunderlich, J. Meijer, C.E. Nebel, Active charge state control of single NV centres in diamond by in-plane Al-schottky junctions, Sci. Rep. 5 (2015), https://doi.org/10.1038/srep12160.

[40] M. Lenzlinger, E.H. Snow, Fowler-Nordheim tunneling into thermally grown SiO2, J. Appl. Phys. 40 (1969) 278, https://doi.org/10.1109/t-ed.1968.16430.

[41] S.D. Subedi, V.V. Federov, D.V. Martyshkin, S.B. Mirov, L. Shao, M. Loncar, Laser spectroscopic characterization of negatively charged nitrogen-vacancy (NV-) centers in diamond, Opt. Mater. Express 9 (2019) 2076–2087, https://doi.org/10.1364/OME.9.002076.

[42] A. Beckel, A. Ludwig, A.D. Wieck, A. Lorke, M. Geller, Time-resolved transconductance spectroscopy on self-assembled quantum dots: spectral evolution from single- into many-particle state, Phys. Rev. B 89 (2014), 155430, https://doi.org/10.1103/PhysRevB.89.155430.